Contribution from the Department of Chemistry,
The University of Calgary, Calgary, Alberta, Canada T2N 1N4

Lewis Base Properties of 1,3-Diphosphadithiatetrazocines: Crystal and Molecular Structures of 1,3-$Ph_4P_2N_4S_2Me^+CF_3SO_3^-$

Tristram Chivers,* Stephen W. Liblong, John F. Richardson, and Tom Ziegler

Received May 10, 1988

The behavior of 1,3-$Ph_4P_2N_4S_2$ toward Lewis and Brønsted acids has been investigated, and the following adducts have been isolated: 1,3-$Ph_4P_2N_4S_2H^+X^-$ (X^- = BF_4^-, $CF_3SO_3^-$), 1,3-$Ph_4P_2N_4S_2Me^+CF_3SO_3^-$, 1,3-$Ph_4P_2N_4S_2$·L (L = BF_3, BCl_3, $SnCl_4$). The progress of the reaction of 1,3-$Ph_4P_2N_4S_2$ with HBF_4 was followed by ^{31}P NMR and UV-visible spectroscopies. All of the adducts exhibit a strong visible absorption band at 365-385 nm and two equally intense signals in the ^{31}P NMR spectrum. An X-ray structural determination of 1,3-$Ph_4P_2N_4S_2Me^+CF_3SO_3^-$ (**3**) showed that the methyl group is coordinated to a nitrogen atom between a phosphorus and a sulfur atom of the $P_2N_4S_2$ ring. The crystals of **3** are monoclinic, space group *Cc*, with a = 15.871 (3) Å, b = 10.566 (2) Å, c = 17.790 (4) Å, β = 91.74 (1)°, V = 2981.9 (7) Å^3, and Z = 4. The final R and R_w values were 0.067 and 0.061, respectively. The planarity of the S_2N_3 unit is retained in **3** with the two phosphorus atoms displaced to the same side of this plane. The angle between the S_2N_3 and PNP planes is 108.1°. The bond lengths involving the coordinated nitrogen are lengthened compared to those of the parent ring system [1.68 vs 1.56 Å for d(S-N) and 1.65 vs 1.61 Å for d(P-N)]. The P-N bond lengths of the PNP unit are unchanged upon coordination while the other S-N bond distances reflect a tendency to form a localized sulfur diimide unit with values of 1.62, 1.53, and 1.52 Å. The geometry around the coordinated nitrogen is essentially planar ($\sum\angle N$ = 359.2°). Ab initio Hartree-Fock-Slater SCF calculations of the electronic and electrostatic components of the protonation energies for the model species 1,3-$H_4P_2N_4S_2H^+$ show that the preference for protonation at a nitrogen between phosphorus and sulfur can be attributed to the dominant electrostatic effects. The conformational changes and hypsochromic shift that occur upon adduct formation are discussed in the context of the calculated electronic structures of the model system 1,3-$H_4P_2N_4S_2$ by using the experimental geometries for 1,3-$Ph_4P_2N_4S_2$ and its methylated derivative.

Introduction

Recently we described a spectroscopic and X-ray structural investigation of some Lewis and Brønsted acid adducts of the phosphadithiatriazine **1** (R = Ph).[1] The major conclusions of

1

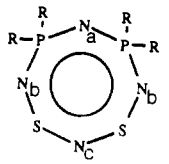

2

that study were that coordination occurs at a nitrogen atom adjacent to the phosphorus atom of the PS_2N_3 ring and is controlled by electrostatic effects. Further it was observed that the S-N bond involving the coordinated nitrogen is weakened substantially and that this nitrogen atom is removed from the planar π-system formed by the other five ring atoms. No evidence for the formation of diadducts of the type **1**·2L was obtained.

We now report similar studies of the Lewis base properties of the homologous eight-membered ring **2** (R = Ph). This heterocycle is a hybrid of the well-known cyclotetraphosphazenes, $(R_2PN)_4$, and cyclotetrathiazene, S_4N_4. The limited structural information available for monoprotonated derivatives of $(Me_2PN)_4$ reveals only small changes in the conformation of the ring and an alternation of P-N bond lengths that cannot be explained by inductive effects alone.[2] The formation of diadducts with HCl has also been observed.[3] Numerous 1:1 adducts of S_4N_4 with Lewis acids, including $S_4N_4H^+$, have been structurally characterized.[4] All of these adducts have a similar structure in which one nitrogen atom is coordinated to the acid and the S_4N_4 ring is flattened into a puckered boat with no S-S cross-ring interaction. Diadducts, e.g. S_4N_4·2$BeCl_2$, have also been reported, but no structural information is available.[5] In contrast to $(R_2PN)_4$ and S_4N_4, there are three possible sites of electrophilic attack, N_a, N_b, or N_c, for **2**. In addition, **2** is a 10-π-electron system[6] and thus may be regarded as intermediate between the electron-precise 8-π-electron ring of $(R_2PN)_4$ and the electron-rich 12-π-electron system of S_4N_4 in terms of occupancy of the π-electron manifold. It was of interest, therefore, to determine the preferred coordination site as well as to assess the structural changes that accompany adduct formation in comparison with those found for the parent binary ring systems and the homologue **1**.

In the initial phase of this study the interactions of **2** (R = Ph) with Lewis and Brønsted acids were monitored by ^{31}P NMR and UV-visible spectroscopies in order to determine the extent of adduct formation. Subsequently, crystalline adducts were isolated and characterized in the reactions of **2** (R = Ph) with HBF_4, HSO_3CF_3, $MeSO_3CF_3$, BCl_3, BF_3 and $SnCl_4$. The structure of 1,3-$(Ph_4P_2N_4S_2)Me^+SO_3CF_3^-$ was determined by X-ray crystallography. Ab initio Hartree-Fock-Slater (HFS) calculations were carried out on the model system 1,3-$H_4P_2N_4S_2H^+$ in order to (a) determine the reason(s) for preferential protonation at a nitrogen between phosphorus and sulfur, (b) compare the electronic structure of the protonated species with that of the parent ring system **2** (R = H), and (c) provide an explanation for the hypsochromic shift in the visible absorption band of **2** upon adduct formation.

Experimental Section

Reagents and General Procedures. All solvents were dried and distilled before use: methylene dichloride (P_2O_5), pentane and diethyl ether (Na), and acetonitrile (CaH_2 and P_2O_5). All reactions and the manipulation of moisture-sensitive products were carried out under an atmosphere of nitrogen (99.99% purity) passed through Ridox, P_2O_5, and silica gel.

1,3-$Ph_4P_2N_4S_2$[6] was prepared according to the literature method. Other chemicals were obtained from Aldrich Chemical Co. and used as received: BCl_3 (1.0 M solution in hexanes), $SnCl_4$ (1.0 M solution in CH_2Cl_2), BF_3·Et_2O, HBF_4·Et_2O, CF_3SO_3H, and CF_3SO_3Me.

Instrumentation. Infrared spectra (4000-400 cm^{-1}) were recorded as Nujol mulls (KBr windows) or KBr pellets on a Nicolet 5DX FT-IR spectrometer. NMR spectra (^1H, ^{13}C and ^{31}P) were recorded on a Varian XL-200 instrument. ^1H and ^{13}C chemical shifts are referenced to $CHCl_3$ and are reported in ppm downfield from Me_4Si. ^{31}P chemical shifts are referenced to external 85% H_3PO_4. Melting points were obtained on

(1) Chivers, T.; Liblong, S. W.; Richardson, J. F.; Ziegler, T. *Inorg. Chem.* **1988**, *27*, 860.
(2) (a) Trotter, J.; Whitlow, S. H.; Paddock, N. L. *J. Chem. Soc., Chem. Commun.* **1969**, 695. (b) Trotter, J.; Whitlow, S. H. *J. Chem. Soc. A* **1970**, 460.
(3) Calhoun, H. P.; Oakley, R. T.; Paddock, N. L.; Trotter, J. *Can. J. Chem.* **1975**, *53*, 2413.
(4) Cordes, A. W.; Marcellus, C. G.; Noble, M. C.; Oakley, R. T.; Pennington, W. T. *J. Am. Chem. Soc.* **1983**, *105*, 6008 and references cited therein.
(5) Roesky, H. W.; Anhaus, J.; Sheldrick, W. S. *Inorg. Chem.* **1984**, *23*, 75.
(6) Burford, N.; Chivers, T.; Richardson, J. F. *Inorg. Chem.* **1983**, *22*, 1482.

0020-1669/88/1327-4344$01.50/0 © 1988 American Chemical Society

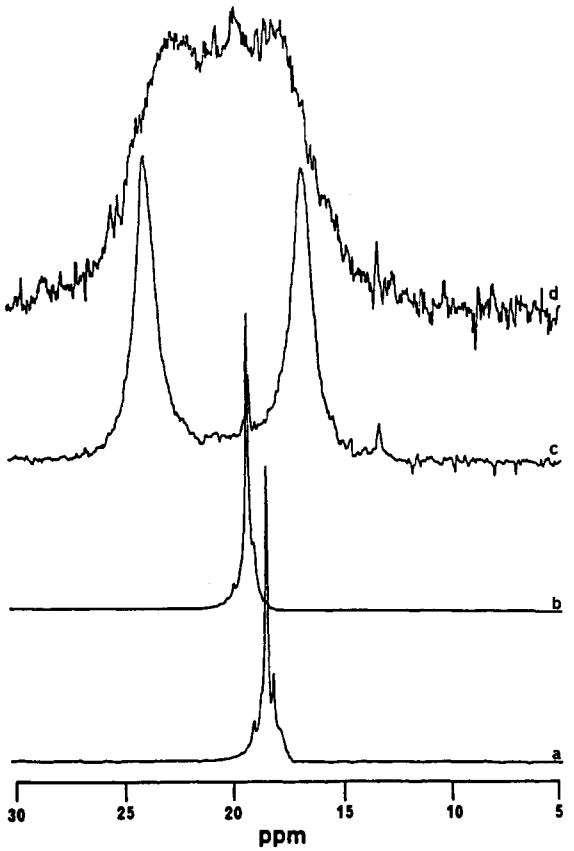

Figure 1. ^{31}P NMR spectra for the reaction of $HBF_4 \cdot Et_2O$ with 1,3-$Ph_4P_2N_4S_2$ recorded at molar ratios of 0:1 (a), 0.6:1 (b), 1.2:1 (c), and 2:1 (d).

samples in open capillary tubes (protected from moisture by Parafilm) and are uncorrected. Chemical analyses were performed by the Analytical Services division of the Department of Chemistry, University of Calgary, and by Guelph Chemical Laboratories Ltd.

Spectroscopic Investigation of the Reaction of 1,3-$Ph_4P_2N_4S_2$ with HBF_4. The course of this reaction was monitored by ^{31}P NMR spectroscopy using the following procedure. A known weight of 1,3-$Ph_4P_2N_4S_2$ was introduced into a septum-sealed 10-mm NMR tube, and a known volume of $CDCl_3$ was added by syringe. This solution was titrated against a solution of $HBF_4 \cdot Et_2O$ in $CDCl_3$ of known concentration by using a calibrated syringe for the addition of the acid, and ^{31}P NMR spectra were recorded for HBF_4:1,3-$Ph_4P_2N_4S_2$ molar ratios of 0:1, 0.6:1, 1.2:1, and 2:1 (see Figure 1). The same reaction was followed by UV–visible spectroscopy using a spectrophotometer cell that was fitted with a rubber septum. A solution of $HBF_4 \cdot Et_2O$ in CH_2Cl_2 of known concentration was added by syringe to a standard solution of 1,3-$Ph_4P_2N_4S_2$ in CH_2Cl_2, and spectra were recorded for the same HBF_4:1,3-$Ph_4P_2N_4S_2$ molar ratios as those used in the NMR experiment. The UV–visible spectra are illustrated in Figure 2.

Preparation of 1,3-$Ph_4P_2N_4S_2H^+BF_4^-$. An excess of $HBF_4 \cdot Et_2O$ (0.21 g, 1.3 mmol) was added by syringe to a stirred solution of 1,3-$Ph_4P_2N_4S_2$ (0.51 g, 1.0 mmol) in 30 mL of diethyl ether. The addition of tetrafluoroboric acid resulted in an immediate decolorization of the orange solution and the production of a yellow precipitate of 1,3-$Ph_4P_2N_4S_2H^+BF_4^-$ (0.57 g, 0.99 mmol), mp 130–132 °C. Anal. Calcd for $C_{24}H_{21}BF_4N_4P_2S_2$: C, 49.84; H, 3.66; N, 9.69. Found: C, 49.04; H, 3.56; N, 10.00. IR (cm^{-1}): 3125 br, w, 1440 s, 1299 m, 1245 vs 1173 vs, 1159 s, 1086 vs, 1068 s, 1023 s, 996 s, 980 m, 885 s, 830 m, 750 m, 742 m, 726 s, 692 vs, 535 vs, 515 s, 500 vs, 428 m. ^1H NMR (in $CDCl_3$): δ 8.00 (1 H, br). UV–visible and ^{31}P NMR spectroscopic data are given in Table I.

Preparation of 1,3-$Ph_4P_2N_4S_2H^+CF_3SO_3^-$. A solution of CF_3SO_3H (0.60 g, 4.0 mmol) in 8 mL of CH_2Cl_2 was added dropwise to a stirred solution of 1,3-$Ph_4P_2N_4S_2$ (0.89 g, 1.8 mmol) in 50 mL of CH_2Cl_2. The solvent was removed under vacuum to give a slightly oily, yellow solid, which was stirred rapidly with diethyl ether (50 mL) for 1 day. The product was separated by filtration and identified as 1,3-$Ph_4P_2N_4S_2H^+CF_3SO_3^-$ (0.98 g, 1.5 mmol), mp 122–124 °C. Anal. Calcd for $C_{25}H_{21}F_3N_4O_3P_2S_3$: C, 46.87; H, 3.30; N, 8.75. Found: C, 46.65; H, 3.41; N, 8.57. IR (cm^{-1}): 3065 w, 2931 br, w, 1440 s, 1293 vs, 1262 vs, 1232 vs, 1223 vs, 1163 vs, 1125 vs, 1026 vs, 997 m, 883 m, 748 m, 728 s, 693 s, 637 vs, 534 vs, 514 s, 496 s. ^1H NMR (in $CDCl_3$): δ 9.31 (1 H, br). UV–visible and ^{31}P NMR spectroscopic data are given in Table I.

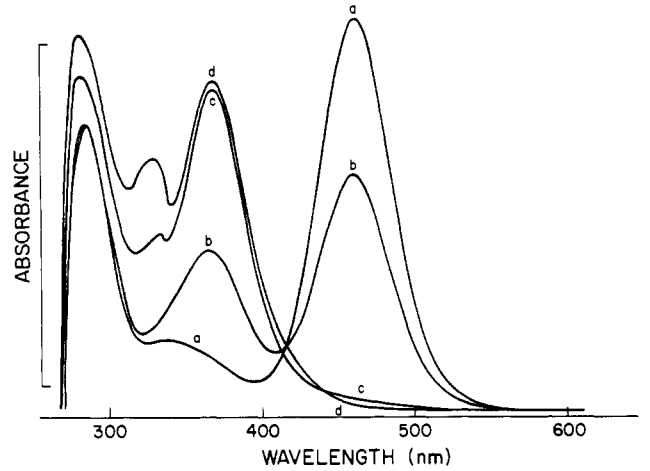

Figure 2. UV–visible spectra for the reaction of $HBF_4 \cdot Et_2O$ with 1,3-$Ph_4P_2N_4S_2$ recorded at molar ratios of 0:1 (a), 0.6:1 (b), 1.2:1 (c), and 2:1 (d).

Table I. Visible Absorption and ^{31}P NMR Spectroscopic Data for Lewis Acid Adducts and Protonated and Methylated Derivatives of 1,3-$Ph_4P_2N_4S_2$

compd	λ_{max} (ϵ)[a,b]	$\delta(^{31}P)$[c]
1,3-$Ph_4P_2N_4S_2H^+BF_4^-$	367 (7×10^3)	23.5, 16.5
1,3-$Ph_4P_2N_4S_2H^+CF_3SO_3^-$	367 (1×10^4)	24.2, 16.7
1,3-$Ph_4P_2N_4S_2Me^+CF_3SO_3^-$	370 (9×10^3)	37.5,[d] 14.4[d]
1,3-$Ph_4P_2N_4S_2 \cdot BCl_3$	384 (8×10^3)	34.5, 12.7
1,3-$Ph_4P_2N_4S_2 \cdot BF_3$	384	32.1, 13.6
1,3-$Ph_4P_2N_4S_2 \cdot SnCl_4$	385	30.8, 16.3
1,3-$Ph_4P_2N_4S_2$[e]	460 (8×10^3)	18.7

[a] In CH_2Cl_2, λ_{max} in nm, ϵ in L mol^{-1} cm^{-1}. [b] Accurate extinction coefficients could not be obtained for the BF_3 and $SnCl_4$ adducts due to dissociation in solution. [c] Chemical shifts relative to 85% H_3PO_4 as external reference. [d] $^2J_{PP}$ = 1.5 Hz. [e] Data taken from ref 6.

Preparation of 1,3-$Ph_4P_2N_4S_2Me_3^+CF_3SO_3^-$. An excess of CF_3SO_3Me (0.38 g, 2.3 mmol) was added by syringe to a stirred solution of 1,3-$Ph_4P_2N_4S_2$ (0.71 g, 1.4 mmol) in 60 mL of diethyl ether, and the mixture was stirred at room temperature for 1 day. The resulting flocculent yellow precipitate was isolated by filtration, dried under vacuum, and identified as 1,3-$Ph_4P_2N_4S_2Me^+CF_3SO_3^-$ (0.90 g, 1.4 mmol) by X-ray crystallography; mp 150–151 °C. Anal. Calcd for $C_{26}H_{23}F_3N_4O_3P_2S_3$: C, 47.70; H, 3.54; N, 8.56. Found: C, 48.05; H, 3.40; N, 8.15. IR (cm^{-1}): 3066 w, 2926 m, 1440 s, 1274 vs, 1260 vs, 1224 s, 1199 s, 1180 vs, 1166 s, 1151 vs, 1118 vs, 1110 s, 1077 m, 1052 s, 1031 vs, 996 s, 853 s, 809 m, 761 m, 755 m, 731 s, 715 m, 707 s, 696 s, 690 s, 637 vs, 542 s, 510 s, 498 s, 445 m, 430 m. ^1H NMR (in $CDCl_3$): δ 2.89 (3 H, d, $^3J_{HP}$ = 9.1 Hz). ^{13}C NMR (in $CDCl_3$): δ 44.1 (CH_3, d, $^2J_{CP}$ = 6.5 Hz). UV–visible and ^{31}P NMR spectroscopic data are given in Table I.

Preparation of 1,3-$Ph_4P_2N_4S_2 \cdot BF_3$. A large excess of $BF_3 \cdot Et_2O$ (1.2 g, 8.5 mmol) was added by syringe to a stirred solution of 1,3-$Ph_4P_2N_4S_2$ (0.74 g, 1.5 mmol) in 40 mL of diethyl ether. This mixture was stirred at 23 °C for 2 h to give a pale orange, microcrystalline product identified as 1,3-$Ph_4P_2N_4S_2 \cdot BF_3$ (0.73 g, 1.3 mmol), mp 110 °C dec. Anal. Calcd for $C_{24}H_{20}BF_3N_4P_2S_2$: C, 51.63; H, 3.61; N, 10.03. Found: C, 51.67; H, 3.73; N, 9.85. IR (cm^{-1}): 1439 vs, 1297 s, 1285 s, 1250 vs, 1172 vs, 1151 vs, 1122 vs, 1110 vs, 1088 vs, 1072 vs, 1024 s, 997 s, 978 s, 938 s, 919 s, 896 vs, 881 vs, 831 m, 810 m, 749 s, 726 vs, 692 vs, 660 m, 539 vs, 501 vs, 472 m, 460 m, 428 s. UV–visible and ^{31}P NMR spectroscopic data are given in Table I.

Preparation of 1,3-$Ph_4P_2N_4S_2 \cdot BCl_3$. A solution of BCl_3 (1.0 M in hexane; 2.2 mmol) was added by syringe to a stirred solution of 1,3-$Ph_4P_2N_4S_2$ (0.99 g, 2.0 mmol) in 50 mL of diethyl ether. The addition of BCl_3 resulted in the immediate decolorization of the orange solution and the production of a pale orange precipitate of 1,3-$Ph_4P_2N_4S_2 \cdot BCl_3$ (1.18 g, 1.94 mmol), mp 110 °C dec. Anal. Calcd for $C_{24}H_{20}BCl_3N_4P_2S_2$: C, 47.44; H, 3.32; N, 9.22. Found: C, 47.28; H, 3.31; N, 8.91. IR (cm^{-1}): 1438 s, 1297 s, 1270 vs, 1162 s, 1122 s, 1113 s, 997 m, 943 vs, 887 vs, 759 m, 749 m, 737 s, 722 s, 713 s, 694 s, 675 s, 595 m, 529 vs, 509 vs, 453 m, 421 m. UV–visible and ^{31}P NMR spectroscopic data are given in Table I.

Table II. Crystallographic Parameters for 1,3-$Ph_4P_2N_4S_2Me^+CF_3SO_3^-$

chem formula: $C_{26}H_{23}F_3N_4O_3P_2S_3$	fw: 654.63
a = 15.871 (3) Å	space group: *Cc* (No. 9)
b = 10.566 (2) Å	T = 23 (1) °C
c = 17.790 (4) Å	λ = 0.71073 Å
β = 91.74 (1)°	ρ_{calcd} = 1.46 g cm^{-3}
V = 2891.9 (7) Å^3	μ = 4.0 cm^{-1}
Z = 4	R = 0.067; R_w = 0.061

Preparation of 1,3-$Ph_4P_2N_4S_2$·$SnCl_4$. An excess of $SnCl_4$ (1.0 M in CH_2Cl_2; 2.0 mmol) was added by syringe to a stirred solution of 1,3-$Ph_4P_2N_4S_2$ (0.45 g, 0.92 mmol) in 30 mL of CH_2Cl_2, and the mixture was stirred at 23 °C for 2 days. The solvent was removed under vacuum, and the yellow solid residue was stirred with *n*-pentane (30 mL) for 1 h. The product was separated by filtration and identified as 1,3-$Ph_4P_2N_4S_2$·$SnCl_4$ (0.59 g, 0.79 mmol), mp 137 °C dec. Anal. Calcd for $C_{24}H_{20}Cl_4N_4P_2S_2Sn$: C, 38.38; H, 2.68; N, 7.46. Found: C, 40.49; H, 2.59; N, 7.13. IR (cm^{-1}): 1438 s, 1295 m, 1262 s, 1181 m, 1121 vs, 1074 m, 1012 m, 998 m, 903 m, 747 m, 728 m, 690 s, 536 m, 525 m, 496 m. UV–visible and ^{31}P NMR spectroscopic data are given in Table I.

X-ray Analysis. Crystals of 1,3-$Ph_4P_2N_4S_2Me^+CF_3SO_3^-$ were obtained from a CH_3CN–diethyl ether solution. The crystal data and experimental details are given in Table II. A yellow crystal of approximate dimensions 0.4 × 0.5 × 0.5 mm was cut from a large crystal and mounted in a glass capillary in a random orientation under nitrogen. Cell constants and an orientation matrix were determined by least-squares refinement of the diffraction geometry of 25 accurately centered reflections ($13 < \theta < 19°$). The choice of space group was confirmed by using the program TRACER[7] and by the successful solution and refinement of the structure. Data were collected at room temperature on an Enraf-Nonius CAD4 automated diffractometer by using the ω–2θ scan technique. As a check on crystal and electronic stability three representative reflections were measured every 60 min. The intensities of these reflections increased an average of 1.8%, so a correction was applied. The data were corrected for Lorentz and polarization effects, and an empirical absorption correction (program DIFABS[8]) was applied to account for the unusual crystal shape and the glass capillary. Details concerning data collection and reduction can be found in ref 9.

The structure was solved by direct methods, which revealed the position of 5 atoms (three S and two P). The remaining atoms were located in succeeding difference Fourier syntheses. Hydrogen atoms, with the exception of those on the CH_3 group and the smaller fragment of the disordered phenyl ring (vide supra), were located and added to the structure factor calculation with isotropic thermal parameters set to $1.3B_{iso}$ of the bonded C atom. H atoms were restrained to "ride" on the bonded atom so H parameters were not refined. Refinement was carried out by full-matrix least-squares on F, minimizing the function $\sum_w(|F_o| - |F_c|)^2$ where the weight w is defined as $4F_o^2/[\sigma^2(F_o^2)]$. The instability factor p was set to 0.04. Scattering factors were taken from Cromer and Waber[10] and anomalous dispersion effects were included in F_c;[11] the values for $\Delta f'$ and $\Delta f''$ were those of Cromer.[12] Refinement of the enantiomeric model showed no significant improvement in the R values, and an isotropic extinction parameter could not be refined.

Two sites of disorder were identified and modeled. The first involved the phenyl ring C(21)–C(26) in which C(21) and C(24) are common to two rings that are at an angle of 47° to each other in a 70:30 ratio. The second disorder consists of rotational motion of the $CF_3SO_3^-$ ion. The CF_3 unit was modeled as a cone with the apex being the C atom and the base consisting of a number of F sites with occupancies varying from 0.2 to 0.7. The SO_3 unit consists of two SO_3 sites of 50% occupancy, which are at 180° to each other and thus share the S and two O atoms. The model converged (the largest Δ/σ being associated with the disordered anion) with final agreement factors of $R = \sum(||F_o| - |F_c||)/\sum|F_o| = 0.067$ and $R_w = [\sum w(|F_o| - |F_c|)^2/\sum w|F_o|^2]^{1/2} = 0.061$. The highest peak in the final difference Fourier had a height of 0.75 e/Å^3 with an error of 0.08 based on $\sigma(F)$[13] and was associated with the disordered CF_3SO_3 anion. Plots of $\sum(|F_o| - |F_c|)^2$ vs $|F_o|$, reflection order in data collection, $(\sin\theta)/\lambda$, and various classes of indices showed no unusual trends. The final atomic coordinates of the non-H atoms of **3** are given in Table III.

Table III. Positional Parameters and B_{eq}[a] for the Non-H Atoms of **3**

atom	x	y	z	B, Å^2	occupancy[b]
S(1)	0.289	0.4634 (2)	0.062	7.67 (3)	
S(2)	0.4046 (1)	0.2366 (2)	0.07125 (9)	6.43 (3)	
P(1)	0.36990 (8)	0.2221 (1)	0.23539 (8)	4.48 (2)	
P(2)	0.22815 (8)	0.3864 (1)	0.20549 (8)	4.44 (2)	
N(1)	0.3511 (5)	0.3474 (8)	0.0409 (4)	7.9 (1)	
N(2)	0.4135 (3)	0.2049 (5)	0.1543 (3)	5.6 (1)	
N(3)	0.2729 (2)	0.2593 (5)	0.2332 (2)	5.17 (8)	
N(4)	0.2850 (3)	0.4840 (5)	0.1549 (3)	5.62 (9)	
C(1)	0.3466 (5)	0.5780 (7)	0.1892 (5)	8.7 (2)	
C(11)	0.4355 (3)	0.3320 (6)	0.2847 (3)	5.2 (1)	
C(12)	0.4132 (4)	0.3679 (8)	0.3583 (3)	6.8 (1)	
C(13)	0.4593 (6)	0.4584 (9)	0.3983 (5)	8.0 (2)	
C(14)	0.5290 (6)	0.513 (1)	0.3627 (6)	9.7 (2)	
C(15)	0.5497 (5)	0.4814 (9)	0.2935 (5)	7.9 (2)	
C(16)	0.5063 (4)	0.3885 (7)	0.2539 (4)	6.5 (1)	
C(21)	0.3760 (4)	0.0698 (5)	0.2801 (3)	5.4 (1)	
C(22)	0.4375 (6)	−0.009 (1)	0.2650 (6)	8.2 (2)	0.7
C(23)	0.4503 (7)	−0.1242 (8)	0.3061 (7)	8.6 (2)	0.7
C(24)	0.3925 (7)	−0.1632 (8)	0.3482 (6)	8.6 (2)	
C(25)	0.322 (1)	−0.085 (1)	0.3662 (7)	11.3 (3)	0.7
C(26)	0.3122 (6)	0.0339 (9)	0.3316 (6)	7.5 (2)	0.7
C(122)	0.454 (2)	0.026 (3)	0.304 (2)	8.1 (6)*	0.3
C(123)	0.447 (3)	−0.077 (5)	0.353 (2)	10.0 (9)*	0.3
C(125)	0.317 (1)	−0.118 (3)	0.311 (1)	7.0 (5)*	0.3
C(126)	0.318 (1)	−0.006 (2)	0.286 (1)	5.7 (3)*	0.3
C(31)	0.1373 (3)	0.3443 (5)	0.1472 (3)	4.66 (9)	
C(32)	0.1228 (3)	0.2197 (6)	0.1328 (4)	5.8 (1)	
C(33)	0.0514 (4)	0.1851 (7)	0.0878 (5)	7.2 (2)	
C(34)	−0.0046 (4)	0.2735 (8)	0.0633 (5)	8.3 (2)	
C(35)	0.0119 (5)	0.3985 (9)	0.0779 (6)	9.2 (2)	
C(36)	0.0831 (4)	0.4350 (6)	0.1222 (5)	6.7 (1)	
C(41)	0.1942 (4)	0.4760 (6)	0.2824 (3)	5.7 (1)	
C(42)	0.1738 (6)	0.6063 (9)	0.2733 (4)	8.3 (2)	
C(43)	0.1455 (8)	0.6726 (9)	0.3367 (6)	14.5 (2)	
C(44)	0.1340 (9)	0.605 (2)	0.4031 (7)	12.9 (3)	
C(45)	0.1500 (7)	0.483 (1)	0.4087 (4)	10.8 (3)	
C(46)	0.1789 (5)	0.4136 (8)	0.3522 (4)	7.4 (1)	
S(3)	0.1572 (1)	0.1785 (2)	0.5608 (2)	9.66 (6)	
C(2)	0.233 (1)	0.095 (2)	0.525 (1)	13.5 (4)*	
F(1)	0.2338 (8)	−0.034 (1)	0.5299 (7)	12.9 (3)*	0.7
F(2)	0.308 (2)	0.117 (3)	0.585 (1)	11.7 (6)*	0.3
F(3)	0.311 (1)	0.111 (2)	0.527 (1)	8.9 (4)*	0.3
F(4)	0.264 (2)	0.004 (3)	0.585 (2)	13.9 (8)*	0.3
F(5)	0.201 (1)	−0.024 (2)	0.494 (1)	8.0 (3)*	0.3
F(6)	0.277	0.166	0.484	9.6 (7)*	0.2
F(7)	0.221	0.125	0.443	8.8 (6)*	0.2
O(1)	0.1808 (6)	0.2957 (6)	0.5836 (5)	11.5 (2)	
O(2)	0.0816 (5)	0.128 (1)	0.5581 (5)	12.6 (2)	
O(3)	0.172 (2)	0.090 (1)	0.6456 (7)	18.1 (5)	0.5
O(4)	0.109	0.188	0.484	20 (1)*	0.5

[a] Starred values denote isotropically refined atoms. Values for anisotropically refined atoms are given in the form of the isotropic equivalent displacement parameter defined as: $(4/3)[a^2B(1,1) + ... + ab(\cos\gamma)B(1,2) + ...]$. [b] Occupancy factors are listed if other than 1.0.

Theoretical Method. All calculations were carried out by utilizing the HFS-LCAO program system developed by Baerends et al.[14] The *ns* and *np* shells on N, P, and S were represented by a double-ζ STO basis set augmented by a 3d STO for P and S (ζ^{P}_{3d} = 1.35, ζ^{S}_{3d} = 1.55). The 1s shell of the H atoms was represented by a double-ζ STO basis set, augmented by a single 2p STO (ζ^{H}_{2p} = 1.0).[15] The electrons in shells of lower energy on N, P, and S were considered as core electrons and were treated by the frozen-core approximation according to the procedure due

(7) Frenz, B. A. "The Enraf-Nonius CAD4 SDP—A Real-time System for Concurrent X-Ray Data Collection and Crystal Structure Determination." In *Computing in Crystallography*; Schenk, H., Olthof-Hazelkamp, R., van Konigsveld, H., Bassi, G. C., Eds.; Delft University Press: Delft, Holland, 1978; pp 64–71.
(8) Walker, N.; Stuart, D. *Acata Crystallogr.* **1983**, *A39*, 159.
(9) Chivers, T.; Richardson, J. F.; Smith, N. R. M. *Inorg. Chem.* **1985**, *24*, 2453.
(10) Cromer, D. T.; Waber, J. T. *International Tables for X-Ray Crystallography*; Kynoch: Birmingham, England, 1974; Vol IV, Table 2.2B.
(11) Ibers, J. A.; Hamilton, W. C. *Acta Crystallogr.* **1964**, *17*, 781.
(12) Reference 8; Table 2.3.1.
(13) Cruickshank, D. W. J. *Acta Crystallogr.* **1949**, *2*, 154.
(14) Baerends, E. J.; Ellis, D. E.; Ros, P. *Chem. Phys.* **1973**, *2*, 41.
(15) (a) Vernooijs, R.; Snijders, J. G.; Baerends, E. J. "Slater type basis functions for the whole periodic system"; Internal Report, The Free University of Amsterdam: Amsterdam, The Netherlands, 1981. (b) Snijders, G. J.; Baerends, E. J.; Vernooijs, P. *At. Data Nucl. Data Tables* **1982**, *26*, 483.

Table IV. Selected Bond Lengths (Å) and Bond Angles (deg) for 1,3-$Ph_4P_2N_4S_2$ (2 (R = Ph)) and 1,3-$Ph_4P_2N_4S_2Me^+CF_3SO_3^-$ (3)[a]

	2 (R = Ph)[b]	3		2 (R = Ph)[b]	3
P(1)–N(3)	1.585 (3)	1.588 (4)	S(2)–N(1)	1.589 (2)	1.535 (8)
P(2)–N(3)	1.585 (3)	1.590 (5)	S(1)–N(1)	1.589 (2)	1.621 (9)
P(1)–N(2)	1.610 (4)	1.625 (5)	P(1)–C(11)	1.814 (5)	1.773 (6)
P(2)–N(4)	1.610 (4)	1.654 (5)	P(1)–C(21)	1.779 (4)	1.797 (6)
N(2)–S(2)	1.562 (4)	1.522 (5)	P(2)–C(31)	1.814 (5)	1.806 (5)
N(4)–S(1)	1.562 (4)	1.677 (5)	P(2)–C(41)	1.799 (4)	1.762 (6)
N(4)–C(1)		1.509 (9)			
N(3)–P(1)–N(2)	118.1 (2)	116.3 (2)	N(4)–S(1)–N(1)	120.2 (2)	111.5 (3)
N(3)–P(2)–N(4)	118.1 (2)	116.7 (2)	S(2)–N(1)–S(1)	144.1 (4)	146.2 (4)
P(1)–N(3)–P(2)	126.0 (3)	129.9 (3)	P(2)–N(4)–C(1)		123.2 (5)
P(1)–N(2)–S(2)	134.5 (2)	143.9 (3)	S(1)–N(4)–C(1)		116.2 (6)
P(2)–N(4)–S(1)	134.5 (2)	119.8 (3)	C(11)–P(1)–C(21)	109.0 (2)	110.1 (3)
N(2)–S(2)–N(1)	120.2 (2)	123.0 (3)	C(41)–P(2)–C(31)	109.0 (2)	108.7 (2)

[a] The atomic numbering scheme is given in Figure 3. [b] Data taken from ref 6.

to Baerends et al.[14] The decomposition of the protonation energies into electronic and electrostatic components was accomplished according to the scheme of Rauk and Ziegler.[16]

Results and Discussion

Spectroscopic Investigation of the Reaction of $HBF_4 \cdot Et_2O$ with 1,3-$Ph_4P_2N_4S_2$ (2 (R = Ph)). In order to gain a detailed picture of adduct formation, the reaction of **2** (R = Ph) with HBF_4 was monitored by ^{31}P NMR spectroscopy and by UV–visible spectroscopy over a range of HBF_4:1,3-$Ph_4P_2N_4S_2$ molar ratios. The ^{31}P NMR spectra for molar ratios of 0:1, 0.6:1, 1.2:1, and 2:1 are shown in Figure 1. These spectra clearly indicate that, as was found for **1** (R = Ph),[1] a rapid exchange process occurs between the protonated and nonprotonated rings. This exchange process is manifested by a single time-averaged signal rather than the appearance of a new signal (or set of signals) for the protonated ring and a concomitant decrease in the intensity of the signal due to **2** (R = Ph). At a molar ratio slightly greater than 1:1 two signals corresponding to the monoprotonated ring are observed (vide supra). When the molar ratio significantly exceeds 1:1, these two signals coalesce to give a very broad signal, indicating that a second, slower exchange process occurs for the addition of a second proton. This signal could not be resolved at higher molar ratios, suggesting that the second proton is weakly bound and/or that diprotonation promotes ring cleavage.

The UV–visible spectra for the HBF_4–1,3-$Ph_4P_2N_4S_2$ reaction at molar ratios of 0:1, 0.6:1, 1.2:1, and 2:1 are shown in Figure 2. Addition of HBF_4 to a solution of **2** (R = Ph) in CH_2Cl_2 results in a decrease in the intensity of the absorption band at 460 nm due to **2** (R = Ph) and the appearance of a new absorption band at 367 nm attributed to the monoprotonated form of **2** (R = Ph). In contrast to the behavior of **1** (R = Ph) upon protonation, only one isobestic point is observed at ca. 410 nm and a second absorption band at ca. 330 nm is present in these solutions. Furthermore, this absorption band does not appear in the UV–visible spectrum of a solution of pure $Ph_4P_2N_4S_2H^+BF_4^-$ and is thus attributed to the diprotonated form $[1,3\text{-}Ph_4P_2N_4S_2H_2^{2+}][BF_4^-]_2$.

Preparation and Spectroscopic Characterization of Lewis Acid Adducts and Protonated and Methylated Derivatives of 2 (R = Ph). The Lewis acid adducts of **2** (R = Ph) with BF_3, BCl_3, or $SnCl_4$ and the protonated or methylated derivatives of **2** (R = Ph) were obtained by addition of an excess of the appropriate reagent to a stirred solution of **2** (R = Ph) in suitable solvents. The adducts were isolated in high yields as moisture-sensitive, yellow-orange precipitates. Only the methylated and protonated salts could be recrystallized without dissociation.

The yellow-orange color of the adducts (λ_{max} = 365–385 nm) is significantly paler than the intense, deep orange color of **2** (R = Ph; λ_{max} = 460 nm) (Table I). The relative strength of the interaction between **2** (R = Ph) and the various acceptors is indicated by the fact that the visible absorption band for the protonated and methylated derivatives is observed at 365–370 nm and no dissociation in solution is evident, whereas the corresponding band for the Lewis acid adducts occurs at ca. 385 nm and the presence of free ligand in solution is readily detected by the appearance of the characteristic band at 460 nm.

The ^{31}P NMR spectra of the adducts of **2** (R = Ph) all show two signals in the ranges of +13 to +17 ppm and +24 to +38 ppm; cf. +19 ppm for **2** (R = Ph) (Table I). The inequivalence of the two phosphorus atoms indicates that the preferred site of attack by these electrophiles is one of the symmetry-related nitrogen atoms, N_b, in **2** (R = Ph) rather than one of the unique nitrogen atoms, N_a or N_c, which lie on the C_2 axis of the ring. Surprisingly, coupling between the two phosphorus atoms could only be resolved for the methylated derivative, which exhibited an uncharacteristically small two-bond coupling constant of $^2J_{pp}$ = 1.5 Hz.[17] The coupling patterns observed in the ^{13}C and ^1H NMR spectra of 1,3-$Ph_4P_2N_4S_2Me^+CF_3SO_3^-$ (**3**) ($^2J_{CP}$ = 6.5 (d), $^3J_{HP}$ = 9.1 (d) Hz) provide further support for the assignment of N_b as the site of coordination. This conclusion was confirmed by the X-ray crystallographic analysis of **3** described below.

^{31}P NMR spectroscopy also provided evidence for the formation of diadducts of **2** (R = Ph) with BCl_3 or $SnCl_4$. The addition of an excess of the appropriate Lewis acid to a solution of 1,3-$Ph_4P_2N_4S_2 \cdot L$ (L = BCl_3, $SnCl_4$) resulted in a decrease in the intensity of the signals for the monoadduct and the appearance of singlets at +29.8 or +24.4 ppm for BCl_3 or $SnCl_4$, respectively, attributed to the symmetrically substituted diadducts. It was also observed that the formation of the diadducts enhanced considerably the susceptibility of the $P_2N_4S_2$ ring to hydrolysis by traces of moisture in the solvent to give $(H_2NPPh_2)_2N^+Cl^-$ ($\delta(^{31}P)$ +20.2 ppm).[18]

X-ray Crystal Structure of 1,3-$Ph_4P_2N_4S_2Me^+CF_3SO_3^-$ (3). The crystal structure of **3** consists of noninteracting $Ph_4P_2N_4S_2Me^+$ and $CF_3SO_3^-$ ions. An ORTEP drawing with the atomic numbering scheme is displayed in Figure 3, and the pertinent endocyclic and exocyclic bond lengths and bond angles are compared with the corresponding values for **2** (R = Ph) in Table IV. The refinement of this structure was hampered by thermal disorder encountered for the $CF_3SO_3^-$ ion and one of the phenyl groups of the cation (see Experimental Section). The effects of this disorder on the structural parameters of the heterocyclic ring are assumed to be minimal in the ensuing discussion.

The coordination of a methyl group to N(4) causes a marked change in the conformation of the PNP segment of the ring compared to that of **2** (R = Ph). The N(2)–S(2)–N(1)–S(1)–N(4) moiety remains planar with the maximum deviation being 0.054 Å for S(1); cf. 0.019 Å for S(1) in **2** (R = Ph). In contrast to **2** (R = Ph), in which N(3) also lies in the molecular plane and P(1) and P(2) are displaced on opposite sides of this plane by 0.697 Å, all atoms of the P(1)–N(3)–P(2) unit in **3** are located on the same side of the N_3S_2 plane. The angle between these two planes is 108.1°.

(16) Ziegler, T.; Rauk, A. *Inorg. Chem.* **1979**, *18*, 1558.

(17) Typical values for $^2J_{pp}$ in unsymmetrically cyclotetraphosphazenes are ca. 40 Hz. Krishnamurthy, S. S.; Sau, A. C.; Woods, M. *Adv. Inorg. Chem. Radiochem.* **1978**, *21*, 80.

(18) Bezman, I. I.; Smalley, J. H. *Chem. Ind. (London)* **1960**, 839.

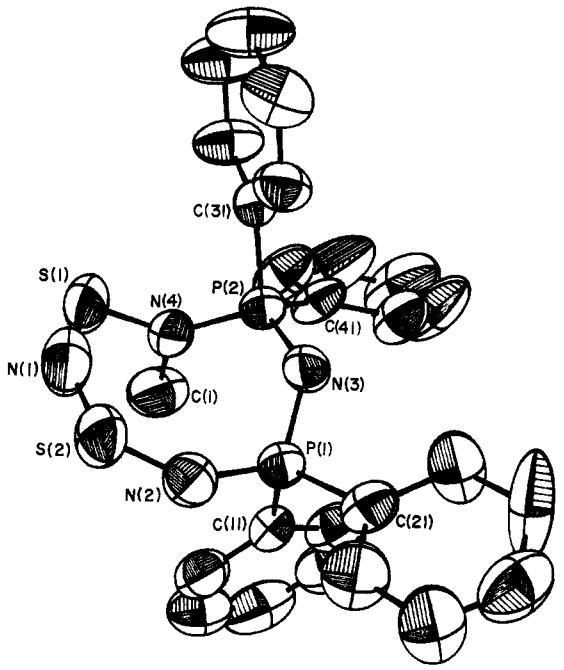

Figure 3. ORTEP plot (50% probability ellipsoids) of the 1,3-$Ph_4P_2N_4S_2Me^+$ cation in **3**.

The observed variations in endocyclic bond lengths for **3** parallel closely those which were found for adducts of **1** (R = Ph).[1] Thus the S(1)–N(4) bond distance is 1.677 (5) Å in **3** compared to 1.562 (4) Å in **2** (R = Ph). The S(1)–N(1) bond length of 1.621 (9) Å is also longer than the corresponding value of 1.589 (2) Å for **2** (R = Ph). The remaining S–N bonds, N(1)–S(2) and S(2)–N(2), are shortened to values in the range of 1.52–1.54 Å, suggesting a tendency toward the formation of a localized four-π-electron system of a sulfur diimide.[19] The changes in the P–N bond lengths are less pronounced. The outer bonds of the N(2)–P(1)–N(3)–P(2)–N(4) unit are only slightly longer (1.63–1.65 Å) than those in **2** (R = Ph), while the inner P–N bonds, which are isolated from the N_3S_2 segment of the ring in **3**, are not altered significantly upon coordination of a methyl group to N(4).

In comparing the structural changes that occur upon methylation of **2** (R = Ph) with those that occur upon methylation of **1** (R = Ph), we note that the elongation of the two S–N bonds nearest to the coordinated nitrogen is less pronounced while the contraction of the S–N bonds in the sulfur diimide unit is greater for **3** compared to that for the methylated derivative of **1** (R = Ph). This observation may be related to the fact that the geometry around the coordinated nitrogen in **3** is essentially planar ($\sum\angle$N(4) = 359.2°) whereas that at the coordinated nitrogen in $Ph_2PN_3S_2Me^+$ is close to tetrahedral, the sum of the angles being 339°.

Regiospecificity of the Methylation of 2 (R = Ph). HFS ab initio molecular orbital calculations for the model ring system 1,3-$H_4P_2N_4S_2$, using the experimental geometry for **2** (R = Ph),[6] indicate that the nitrogen atoms, N_b, connected to phosphorus and sulfur carry a larger negative charge than the unique nitrogen atoms, N_a or N_c ($q(N_a) = -0.18$, $q(N_b) = -0.27$, and $q(N_c) = -0.12$). Consequently, the preferred site of attack by an electrophile on **2** (R = Ph) is expected to be an N_b atom if electrostatic effects are dominant in this interaction, as was found in the case of **1** (R = Ph).[1] The spectroscopic and crystallographic results described above demonstrate that the reaction of **2** (R = Ph) with Lewis or Brønsted acids occurs exclusively at N_b for the formation of both mono- and diadducts. In order to assess the relative importance of electronic or electrostatic effects in determining the regiospecificity of these reactions, we have carried out an analysis of the interaction energies for the model systems 1,3-$H_4P_2N_4S_2H^+$ in which the proton is attached to either N_a (**4**), N_b (**5**), or N_c (**6**), with ab initio HFS–SCF calculations. The calculations were carried out for an N–H distance of 1.0 Å (cf. ref 1), with the proton lying in the molecular plane, by using the experimental geometry for **2** (R = Ph).[6]

Table V. Electrostatic and Electronic Energy Contributions to the Total Interaction Energy of 1,3-$H_4P_2N_4S_2H^+$ (**4–6**)[a]

	$\Delta E_{electrostatic}$[b]	$\Delta E_{electronic}$[c]	ΔE_{total}
4	−3	−197	−200
5	−19	−187	−206
6	+7	−191	−184

[a] In kcal mol^{-1}. [b] The electrostatic interaction energy between H^+ and the ring system of the protonated species. [c] The stabilization energy associated with charge rearrangements in the protonation process.

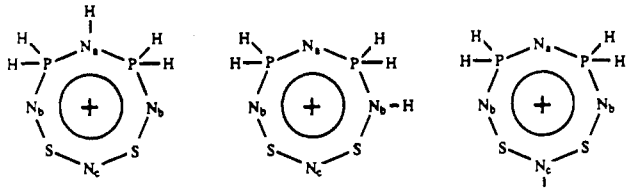

4 **5** **6**

The calculated electrostatic and electronic contributions to the interaction energies of **4–6** are given in Table V. The electrostatic part of the protonation energy represents the Coulomb interaction between H^+ and **2** (R = H), whereas the electronic part is associated with charge rearrangements in the protonation process. It is evident from Table V that the electronic energy contribution to the total interaction energy for protonation at N_b (**5**) in similar to that for protonation at N_c (**6**), whereas the electrostatic contribution is significantly larger for **5** compared to that for **6** (in fact, the electrostatic interaction between N_c and a proton is a destabilizing effect). This difference is analogous to that observed for **1** (R = Ph) and is perhaps not surprising in view of the similarity in the electronic structures of the S_2N_3 units of the ring systems **1** and **2**.[5] Although the electronic energy contribution to the interaction energy for protonation at N_a is significantly larger than that for protonation at N_b, model **5** is seen to be more stable than **4** due to a substantially greater electrostatic energy contribution.

The observed preference for monoadduct formation of N_b is consistent with calculated atomic charge densities for the N atoms in **2** (R = H). Furthermore, the observation that diadduct formation occurs in a symmetrical fashion (i.e. coordination to the second N_b atom) is in agreement with the calculated atomic charge densities for the noncoordinated nitrogen atoms in **5** ($q(N_a) = -0.21$, $q(N_b) = -0.27$, $q(N_c) = 0.22$).

Geometry of the Protonated Ring (5). Previous extended Hückel calculations for **2** (R = H) indicated that this eight-membered ring could be described as an internal salt, $(H_2P{=}N^+{=}PH_2)(S_2N_3^-)$, in which the $S_2N_3^-$ unit accommodates 8 π-electrons (cf. **1**, $H_2P^+S_2N_3^-$)[20] and the $H_2P{=}N^+{=}PH_2$ unit possesses 2 π-electrons.[6] It was noted above that both the pattern of bond length variations and the conformational changes that occur on methylation of **2** (R = Ph) are different from those observed in adducts of **1** (R = Ph). The fact that the planarity of the S_2N_3 unit is retained in 1,3-$Ph_4P_2N_4S_2Me^+$ suggests that the structural changes associated with the coordination of an electrophile to N_b might be best interpreted by a consideration of the internal salt model.

An examination of the results of the interaction of N_b in **2** (R = H) with a proton reveals that, as expected, this interaction involves those orbitals on N_b that are energetically and directionally disposed to interact with the 1s orbital of the approaching proton, i.e. the "high-lying" lone-pair orbitals on N_b. However, in addition to exhibiting lone-pair characteristics, the orbital of **2** (R = H) that is the primary contributor to this interaction also provides a significant bonding contribution to the P–N_b bonds that link

(19) Typical S–N bond lengths in a *cis,cis*-sulfur diimide are ca. 1.52 Å: Gieren, A.; Betz, H.; Hubner, T.; Lamm, V.; Herberhold, M.; Guldner, K. *Z. Anorg. Allg. Chem.* **1984**, *513*, 160.

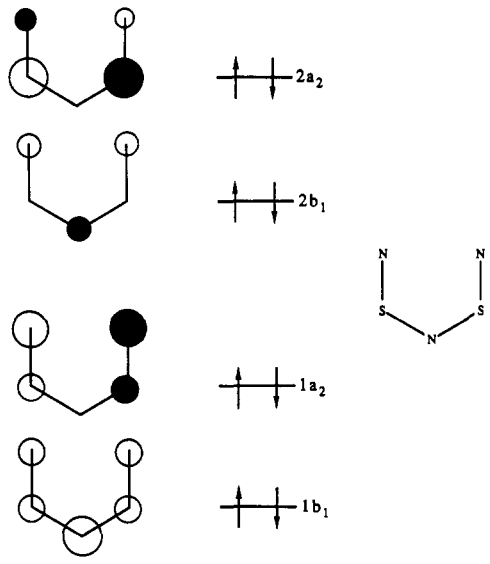

Figure 4. Composition and relative energies of the occupied π-orbitals of $S_2N_3^-$.

the PNP and S_2N_3 units. Thus the evolution of this orbital into the strongly localized N–H σ-bond leads to a weakening of the P–N_b bonds (especially the bond associated with the coordinated nitrogen). The withdrawal of electron density from N_b by the proton should also weaken the P–N_a bond nearest the coordinated nitrogen, but this effect appears to be offset by the conformational change that results in the displacement of the PN_aP unit of the plane of the S_2N_3 segment of the ring.

Studies of the Lewis base properties of other π-electron-rich heterocycles, $S_3N_3^-$,[21] S_4N_4,[4] and **1** (R = Ph),[20] have shown that the bonding of a proton to an endocyclic nitrogen results in a withdrawal of charge from the σ-system away from nitrogen into the N–H bond. Concomitantly there is a migration of π-electron density toward the coordinated nitrogen. It seems reasonable to expect a similar redistribution of electron density upon protonation of the $S_2N_3^-$ unit of **2**. The composition of the four occupied π-orbitals of $S_2N_3^-$ is illustrated in Figure 4. The migration of π-electron density toward the coordinated nitrogen, N_b, is expected to have its greatest effect on the $2a_2$ orbital, although this would be partially offset by the perturbation of the $1a_2$ orbital. The primary effect of protonation at N_b, with respect to the π-system, is expected to be a slight strengthening of the S–N_b π-bond due to a reduced contribution from $2a_2$ to the total bond order. Consistent with this prediction, we note that the elongation of the S–N_b(CH_3) bond is less pronounced and the contraction of the other S–N_b bond is greater in **3** compared to the corresponding values for the methylated derivative of **1** (R = Ph).

Electronic Spectra of Lewis Acid Adducts of 2 (R = Ph). All the adducts of **2** (R = Ph) exhibit an intense visible absorption band at 365–385 nm (Table I). The strong visible absorption band at 460 nm for **2** (R = Ph) has been assigned to the π^*(HOMO) $\rightarrow$ π^*(LUMO) electronic transition.[6] The narrow HOMO–LUMO gap in **2** (R = Ph) arises from a stabilization of the HOMO, and predominantly, LUMO orbitals of the $S_2N_3^-$ unit via d_π–p_π interaction with the d_π orbitals of the $R_2P{=}N^+{=}PR_2$ unit.[6] The conformational change associated with adduct formation by **2**, as exemplified in $Ph_4P_2N_4S_2Me^+$, will reduce the ability of these two π-systems to interact, thereby diminishing the stabilization of the HOMO and, to a greater extent, the LUMO. The hypsochromic shift observed upon adduct formation is consistent with this expectation.

Conclusion. The interaction of 1,3-$Ph_4P_2N_4S_2$ with Lewis or Brønsted acids occurs at one of the nitrogen atoms connected to phosphorus and sulfur and is controlled by electrostatic effects. Coordination to an electrophile imposes a marked perturbation on both the conformation of the ring and the endocyclic bond lengths. The bonds associated with the coordinated nitrogen are weakened substantially, but the S_2N_3 unit in the methylated derivative remains planar so that the contribution of the coordinated nitrogen to the π-system is maintained. Although the effects of the electrophile on the electronic structure of the ring appear to parallel those found for S_4N_4, the structural changes that occur are different due to the presence of Ph_2P groups. In contrast to the behavior of S_4N_4 and $(R_2PN)_4$, the interaction between monoadducts of **2** (R = Ph) and a second electrophile is very weak. As is the case with S_4N_4,[4] however, this interaction does promote breakdown of the ring. This tendency can be attributed to a more pronounced destabilization of the π-electron-rich system in PNS and SN rings compared to the π-electron precise system of cyclophosphazenes.

Acknowledgment. We thank the NSERC (Canada) for financial support in the form of operating and infrastructure grants and a postgraduate scholarship to S.W.L. and Dr. K. A. Kerr for the use of the X-ray diffractometer.

Supplementary Material Available: Tables listing crystallographic parameters, anisotropic thermal parameters, positional and isotropic thermal parameters for H atoms, all bond lengths and bond angles for non-H atoms, and least-squares planes (10 pages); a table of calculated and observed structure factors (8 pages). Ordering information is given on any current masthead page.

(20) Burford, N.; Chivers, T.; Cordes, A. W.; Laidlaw, W. G.; Noble, M.; Oakley, R. T.; Swepston, P. N. *J. Am. Chem. Soc.* **1982**, *104*, 1282.
(21) Marcellus, C. G.; Oakley, R. T.; Cordes, A. W.; Pennington, W. T. *Can. J. Chem.* **1984**, *62*, 1822.